On the dynamic behavior of bladed disks using wave finite element strategies and model reduction techniques

Jean-Mathieu Mencik, Pouloumdé Nikiema, Moustapha Mbaye

On the dynamic behavior of bladed disks using wave finite element strategies and model reduction techniques

J.-M. Mencik [1], **P. Nikiema** [1], **M. Mbaye** [2]
[1] INSA Centre Val de Loire, Université d'Orléans, Université de Tours,
Laboratoire de Mécanique Gabriel Lamé,
Rue de la Chocolaterie, 41000 Blois, France
e-mail: **jean-mathieu.mencik@insa-cvl.fr**

[2] Safran Tech, Digital Sciences & Technologies Department,
Rue des Jeunes Bois, Châteaufort, 78114 Magny-Les-Hameaux, France

Abstract
In this paper the wave finite element method is applied to compute the harmonic response of bladed disks with distributed loads, e.g., for substructures (sectors) subjected to an engine order excitation. The proposed approach consists in (i) expressing the displacements and forces at the interfaces between the substructures in terms of wave modes, (ii) expressing the external forces in terms of wave modes and (iii) solving a local/substructure equation for expressing wave amplitudes. To improve the efficiency of the WFE method, a model reduction technique is proposed where the key idea is to express the displacement vectors at the substructure interfaces with a small number of boundary modes. Numerical simulations are carried out on a 3D industrial structure where the efficiency and accuracy of the WFE approach are demonstrated.

1 Introduction

Bladed disks are common components in industrial gas turbine aero-engines or power generation turbines, e.g., compressor or turbine bladed disks subjected to an engine order (EO) excitation resulting from aerodynamic wakes and potential effects. Predicting their dynamic behavior by means of accurate and efficient numerical tools has become a key challenge which is motivated by the need of considering systems with increasing complexity, i.e., for sectors/substructures with many internal and interface degrees of freedom (DOFs). In this case, the standard finite element (FE) procedure requires high computational resources due to the element assembly procedure and the resolution of large-sized matrices.

To address the modeling of bladed disks subjected to harmonic external forces, the wave finite element (WFE) method can be used as an efficient alternative to the standard FE method. Within the WFE framework, wave modes in periodic structures are determined by computing the eigenvalues and eigenvectors of the transfer matrix of a substructure, see [1, 2, 3]. To assess the harmonic forced response of 1D-periodic structures — i.e., structures consisting of the repetition of identical substructures along a straight or circumferential direction —, the WFE method involves expanding the displacement and force vectors at the interfaces between the substructures on a wave mode basis (i.e., using the eigenvectors of the transfer matrix). Concerning structures with cyclic symmetry like bladed disks, the reader is referred to [4, 5, 6]. Also, the analysis of 1D-periodic structures with distributed external forces has been investigated in [7, 8] where the external forces are expressed in terms of wave modes in the same way as the displacement and force vectors at the substructure interfaces.

In the present paper, a WFE approach is proposed which combines previous works from the literature [5, 8]. The focus is on predicting the dynamic behavior of bladed disks subjected to distributed loads (engine order excitation), e.g., circumferential forces applied at the tips of the blades as shown in Fig. 1. In a nutshell, the proposed approach consists in (i) expressing the displacements and forces at the interfaces between the

substructures in terms of wave modes, (ii) expressing the external forces in terms of wave modes and (iii) solving a local/substructure equation for expressing wave amplitudes.

For substructures with many internal and interface DOFs, the WFE method raises numerical challenges like (i) the condensation of the internal DOFs of a substructure onto its interface DOFs and (ii) the computation of a large eigenproblem associated with the interface DOFs. To tackle these issues, model reduction techniques are proposed in this paper. First, a reduction for the internal DOFs is performed using the Craig-Bampton (CB) method [9]. Next, an interface reduction is considered where the displacement vectors at the substructure interfaces are expressed with a small number of boundary modes [10, 11]. With this strategy, the wave modes can be efficiently computed by solving a small eigenproblem. To control the accuracy of the proposed model reduction techniques, an original error indicator that considers a force balance equation at the substructure interfaces is proposed.

The proposed WFE approach focuses on the dynamic analysis of bladed disks like those encountered in industrial applications where the substructures (sectors) contain many internal and interface DOFs. Also, it focuses on the analysis of mistuned bladed disks, i.e., bladed disks containing a few perturbed substructures.

The rest of the paper is organized as follows. In Sec. 2, the strategies for modeling tuned (i.e., purely periodic) and mistuned bladed disks subjected to harmonic external forces are presented. In Sec. 3, model reduction techniques are discussed. Also, in this section, an error indicator is proposed to control the accuracy of the model reduction strategy. In Sec. 4, numerical simulations are carried out on a 3D industrial structure where the efficiency and accuracy of the WFE approach are discussed.

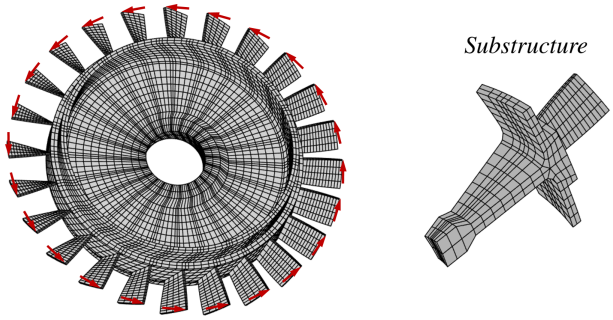

Figure 1: (Left) FE mesh of a bladed disk with external forces at the tips of the blades. (Right) FE mesh of a substructure.

2 WFE method

2.1 Substructure modeling

Bladed disks are periodic structures with cyclic symmetry, i.e., structures made up of identical substructures (say, N substructures) which are meshed in the same way in a cylindrical coordinate system with angular period $\Delta\theta = 2\pi/N$. To make it more concrete, a simple periodic structures with 2D substructures is shown in Fig. 2 where the tips of the substructures are subjected to tangential forces.

A substructure enclosed between two interfaces (N) and (1) is shown in Fig. 2. Here, the boundary DOFs, corresponding with these interfaces, are denoted as Γ_- and Γ_+ (where the assumption is made that these interfaces are meshed with the same number n of DOFs), while the other "internal" DOFs are denoted as $\mathtt{I}$. Let us denote by $\mathbf{q}$ and $\mathbf{F}$ the displacement and force vectors of this substructure, and by $\mathbf{D}$ the dynamic stiffness matrix of the substructure (similar for all the substructures) expressed as $\mathbf{D} = -\omega^2\mathbf{M} + \mathtt{i}\omega\mathbf{C} + \mathbf{K}$ with $\mathbf{M}$, $\mathbf{C}$ and $\mathbf{K}$ the mass, damping and stiffness matrices (respectively), ω the frequency and $\mathtt{i}$ the

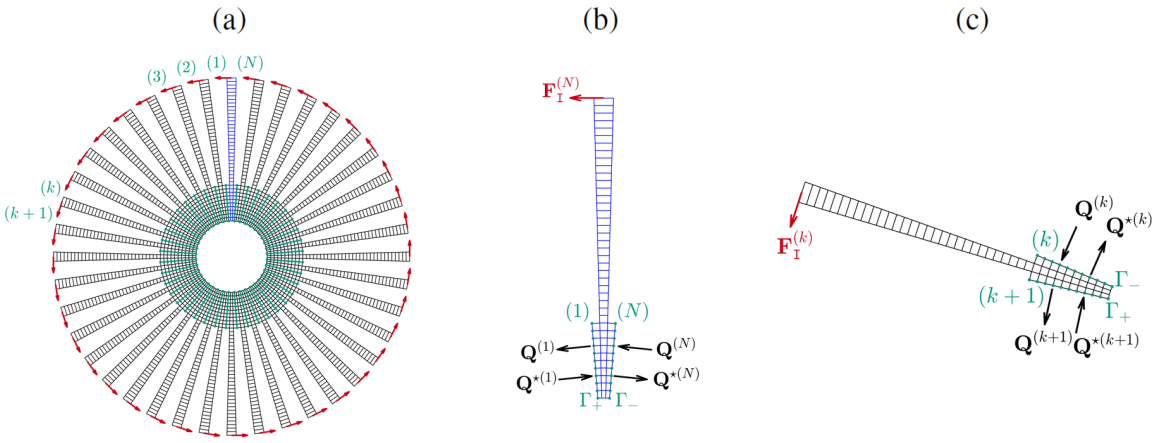

Figure 2: Schematics of (a) a periodic structure with cyclic symmetry and 2D substructures, (b) a substructure enclosed between interfaces (N) and (1) and (c) a substructure enclosed between interfaces (k) and $(k+1)$.

imaginary unit. Then, in the frequency domain, the dynamic equation of the substructure writes:

$$\mathbf{D}\mathbf{q} = \mathbf{F} \quad \Rightarrow \quad \begin{bmatrix} \mathbf{D}_{\Gamma_-\Gamma_-} & \mathbf{D}_{\Gamma_-\mathrm{I}} & \mathbf{D}_{\Gamma_-\Gamma_+} \\ \mathbf{D}_{\mathrm{I}\Gamma_-} & \mathbf{D}_{\mathrm{II}} & \mathbf{D}_{\mathrm{I}\Gamma_+} \\ \mathbf{D}_{\Gamma_+\Gamma_-} & \mathbf{D}_{\Gamma_+\mathrm{I}} & \mathbf{D}_{\Gamma_+\Gamma_+} \end{bmatrix} \begin{bmatrix} \mathbf{q}_{\Gamma_-}^{(N)} \\ \mathbf{q}_{\mathrm{I}}^{(N)} \\ \mathbf{q}_{\Gamma_+}^{(1)} \end{bmatrix} = \begin{bmatrix} \mathbf{F}_{\Gamma_-}^{(N)} \\ \mathbf{F}_{\mathrm{I}}^{(N)} \\ \mathbf{F}_{\Gamma_+}^{(1)} \end{bmatrix}, \tag{1}$$

where $\mathbf{F}_{\Gamma_-}^{(N)}$ and $\mathbf{F}_{\Gamma_+}^{(1)}$ represent the vectors of coupling forces at the interfaces with the connected substructures, and $\mathbf{F}_{\mathrm{I}}^{(N)}$ represents the vector of external forces. By condensing the internal DOFs of the substructure onto the boundary/interface ones, Eq. (1) gives:

$$\mathbf{D}^*\mathbf{q}_\Gamma = \mathbf{F}_\Gamma + \mathbf{F}_{\mathrm{I}}^{*(N)} \quad \Leftrightarrow \quad \begin{bmatrix} \mathbf{D}^*_{\Gamma_-\Gamma_-} & \mathbf{D}^*_{\Gamma_-\Gamma_+} \\ \mathbf{D}^*_{\Gamma_+\Gamma_-} & \mathbf{D}^*_{\Gamma_+\Gamma_+} \end{bmatrix} \begin{bmatrix} \mathbf{q}_{\Gamma_-}^{(N)} \\ \mathbf{q}_{\Gamma_+}^{(1)} \end{bmatrix} = \begin{bmatrix} \mathbf{F}_{\Gamma_-}^{(N)} \\ \mathbf{F}_{\Gamma_+}^{(1)} \end{bmatrix} + \begin{bmatrix} \mathbf{F}_{\mathrm{I}}^{*(N)}|_{\Gamma_-} \\ \mathbf{F}_{\mathrm{I}}^{*(N)}|_{\Gamma_+} \end{bmatrix}. \tag{2}$$

where:

$$\mathbf{D}^* = \begin{bmatrix} \mathbf{D}^*_{\Gamma_-\Gamma_-} & \mathbf{D}^*_{\Gamma_-\Gamma_+} \\ \mathbf{D}^*_{\Gamma_+\Gamma_-} & \mathbf{D}^*_{\Gamma_+\Gamma_+} \end{bmatrix} = \begin{bmatrix} \mathbf{D}_{\Gamma_-\Gamma_-} & \mathbf{D}_{\Gamma_-\Gamma_+} \\ \mathbf{D}_{\Gamma_+\Gamma_-} & \mathbf{D}_{\Gamma_+\Gamma_+} \end{bmatrix} - \begin{bmatrix} \mathbf{D}_{\Gamma_-\mathrm{I}} \\ \mathbf{D}_{\Gamma_+\mathrm{I}} \end{bmatrix} \mathbf{D}_{\mathrm{II}}^{-1} \begin{bmatrix} \mathbf{D}_{\mathrm{I}\Gamma_-} & \mathbf{D}_{\mathrm{I}\Gamma_+} \end{bmatrix}, \tag{3}$$

and

$$\mathbf{F}_{\mathrm{I}}^{*(N)} = \begin{bmatrix} \mathbf{F}_{\mathrm{I}}^{*(N)}|_{\Gamma_-} \\ \mathbf{F}_{\mathrm{I}}^{*(N)}|_{\Gamma_+} \end{bmatrix} = - \begin{bmatrix} \mathbf{D}_{\Gamma_-\mathrm{I}} \\ \mathbf{D}_{\Gamma_+\mathrm{I}} \end{bmatrix} \mathbf{D}_{\mathrm{II}}^{-1} \mathbf{F}_{\mathrm{I}}^{(N)}. \tag{4}$$

After some simple algebra, Eq. (2) leads to:

$$\mathbf{u}^{(1)} = \mathbf{S}\mathbf{u}^{(N)} + \mathbf{b}^{(N)}. \tag{5}$$

Here, $\mathbf{u}^{(1)}$ and $\mathbf{u}^{(N)}$ are state vectors expressed by:

$$\mathbf{u}^{(1)} = \begin{bmatrix} \mathbf{q}_{\Gamma_+}^{(1)} \\ \mathbf{F}_{\Gamma_+}^{(1)} \end{bmatrix} = \begin{bmatrix} \mathbf{q}_{\Gamma_-}^{(1)} \\ -\mathbf{F}_{\Gamma_-}^{(1)} \end{bmatrix} \quad , \quad \mathbf{u}^{(N)} = \begin{bmatrix} \mathbf{q}_{\Gamma_-}^{(N)} \\ -\mathbf{F}_{\Gamma_-}^{(N)} \end{bmatrix} = \begin{bmatrix} \mathbf{q}_{\Gamma_+}^{(N)} \\ \mathbf{F}_{\Gamma_+}^{(N)} \end{bmatrix}, \tag{6}$$

In Eq. (5), $\mathbf{S}$ represents the transfer matrix of the substructure expressed by [5]:

$$\mathbf{S} = \begin{bmatrix} -(\mathbf{D}^*_{\Gamma_-\Gamma_+})^{-1}\mathbf{D}^*_{\Gamma_-\Gamma_-} & -(\mathbf{D}^*_{\Gamma_-\Gamma_+})^{-1} \\ \mathbf{D}^*_{\Gamma_+\Gamma_-} - \mathbf{D}^*_{\Gamma_+\Gamma_+}(\mathbf{D}^*_{\Gamma_-\Gamma_+})^{-1}\mathbf{D}^*_{\Gamma_-\Gamma_-} & -\mathbf{D}^*_{\Gamma_+\Gamma_+}(\mathbf{D}^*_{\Gamma_-\Gamma_+})^{-1} \end{bmatrix}. \tag{7}$$

Also, in Eq. (5), $\mathbf{b}^{(N)}$ is a vector that results from the external forces expressed by:

$$\mathbf{b}^{(N)} = -\begin{bmatrix} \mathbf{0} \\ \mathbf{F}_{\mathtt{I}}^{*(N)}|_{\Gamma_+} \end{bmatrix} + \begin{bmatrix} \mathbf{D}_{\Gamma_-\Gamma_+}^{*-1}\mathbf{F}_{\mathtt{I}}^{*(N)}|_{\Gamma_-} \\ \mathbf{D}_{\Gamma_+\Gamma_+}^{*}\mathbf{D}_{\Gamma_-\Gamma_+}^{*-1}\mathbf{F}_{\mathtt{I}}^{*(N)}|_{\Gamma_-} \end{bmatrix}. \tag{8}$$

Eq. (5) represents a relation between the state vectors $\mathbf{u}^{(N)}$ and $\mathbf{u}^{(1)}$, i.e., displacement and force vectors between the interfaces (N) and (1). Similarly, for a substructure enclosed between two arbitrary interfaces (k) and $(k+1)$ (see Fig. 2), the relation writes:

$$\mathbf{u}^{(k+1)} = \mathbf{S}\mathbf{u}^{(k)} + \mathbf{b}^{(k)}. \tag{9}$$

2.2 Free wave propagation

Free waves that travel in forward- and backward-directions around a periodic structure can be assessed from the eigensolutions of the transfer matrix $\mathbf{S}$. Specifically the eigenvalues of $\mathbf{S}$ — namely, μ_j — are wave parameters of the form $\mu_j = \mathtt{exp}(-\mathtt{i}\beta_j\Delta\theta)$ with β_j the circumferential wave numbers; also, the eigenvectors of $\mathbf{S}$ — namely, $\boldsymbol{\phi}_j = [\boldsymbol{\phi}_{\mathtt{q}j}^T \; \boldsymbol{\phi}_{\mathtt{F}j}^T]^T$ — are wave shape vectors with displacement and force components $\boldsymbol{\phi}_{\mathtt{q}j}$ and $\boldsymbol{\phi}_{\mathtt{F}j}$.

It can be proven that the transfer matrix $\mathbf{S}$ of the substructures is symplectic [3], which means that paired eigenvalues $(\mu_j, 1/\mu_j)$ are obtained. This yields n forward-going "wave modes" $(\mu_j, \boldsymbol{\phi}_j)$ with $|\mu_j| < 1$, and n backward-going "wave modes" $(\mu_j^\star, \boldsymbol{\phi}_j^\star)$ with $\mu_j^\star = 1/\mu_j$ and $|\mu_j^\star| > 1$. For computational purposes, the wave modes can be accurately computed via the $\mathbf{S} + \mathbf{S}^{-1}$ transformation proposed in [12]. In matrix notations, the wave parameters and wave shape vectors write:

$$\boldsymbol{\mu} = \mathtt{diag}_{j=1}^{n}\{\mu_j\} \qquad , \qquad \boldsymbol{\mu}^\star = \boldsymbol{\mu}^{-1}, \tag{10}$$

$$\boldsymbol{\Phi} = \begin{bmatrix} \boldsymbol{\Phi}_{\mathtt{q}} \\ \boldsymbol{\Phi}_{\mathtt{F}} \end{bmatrix} \qquad \text{with} \qquad \boldsymbol{\Phi}_{\mathtt{q}} = [\boldsymbol{\phi}_{\mathtt{q}1} \cdots \boldsymbol{\phi}_{\mathtt{q}n}] \qquad \text{and} \qquad \boldsymbol{\Phi}_{\mathtt{F}} = [\boldsymbol{\phi}_{\mathtt{F}1} \cdots \boldsymbol{\phi}_{\mathtt{F}n}], \tag{11}$$

and

$$\boldsymbol{\Phi}^\star = \begin{bmatrix} \boldsymbol{\Phi}_{\mathtt{q}}^\star \\ \boldsymbol{\Phi}_{\mathtt{F}}^\star \end{bmatrix} \qquad \text{with} \qquad \boldsymbol{\Phi}_{\mathtt{q}}^\star = [\boldsymbol{\phi}_{\mathtt{q}1}^\star \cdots \boldsymbol{\phi}_{\mathtt{q}n}^\star] \qquad \text{and} \qquad \boldsymbol{\Phi}_{\mathtt{F}}^\star = [\boldsymbol{\phi}_{\mathtt{F}1}^\star \cdots \boldsymbol{\phi}_{\mathtt{F}n}^\star], \tag{12}$$

where $\boldsymbol{\Phi}_{\mathtt{q}}$, $\boldsymbol{\Phi}_{\mathtt{q}}^\star$, $\boldsymbol{\Phi}_{\mathtt{F}}$ and $\boldsymbol{\Phi}_{\mathtt{F}}^\star$ are $n \times n$ matrices. Finally note that the wave modes possess orthogonality properties [3], i.e., $\boldsymbol{\Phi}^T\mathbf{J}\boldsymbol{\Phi} = \mathbf{0}$, $\boldsymbol{\Phi}^{\star T}\mathbf{J}\boldsymbol{\Phi}^\star = \mathbf{0}$, $\boldsymbol{\Phi}^{\star T}\mathbf{J}\boldsymbol{\Phi} = \mathtt{diag}_{j=1}^{n}\{\boldsymbol{\phi}_j^{\star T}\mathbf{J}\boldsymbol{\phi}_j\}$ and $\boldsymbol{\Phi}^T\mathbf{J}\boldsymbol{\Phi}^\star = \mathtt{diag}_{j=1}^{n}\{\boldsymbol{\phi}_j^T\mathbf{J}\boldsymbol{\phi}_j^\star\}$ where:

$$\mathbf{J} = \begin{bmatrix} \mathbf{0} & \mathbf{I}_n \\ -\mathbf{I}_n & \mathbf{0} \end{bmatrix}. \tag{13}$$

2.3 Forced response

Within the WFE framework, a wave mode expansion for the state vectors $\mathbf{u}^{(k)}$ $(k = 1, \ldots, N)$ is considered as follows [13]:

$$\mathbf{u}^{(k)} = \boldsymbol{\Phi}\mathbf{Q}^{(k)} + \boldsymbol{\Phi}^\star\mathbf{Q}^{\star(k)}, \tag{14}$$

where $\mathbf{Q}^{(k)}$ and $\mathbf{Q}^{\star(k)}$ are wave amplitude vectors. A wave mode expansion for the vectors $\mathbf{b}^{(k)}$ $(k = 1, \ldots, N)$ in Eq. (9) can also be proposed [7]:

$$\mathbf{b}^{(k)} = \boldsymbol{\Phi}\mathbf{Q}_{\mathtt{b}}^{(k)} + \boldsymbol{\Phi}^\star\mathbf{Q}_{\mathtt{b}}^{\star(k)}, \tag{15}$$

where $\mathbf{Q}_{\mathtt{b}}^{(k)}$ and $\mathbf{Q}_{\mathtt{b}}^{\star(k)}$ represent additional wave amplitude vectors. Note that the vectors of external forces $\mathbf{F}_{\mathtt{I}}^{*(k)}$ are known by assumption and, therefore, the vectors $\mathbf{b}^{(k)}$ can be determined, see Eq. (8). Then, by considering the orthogonality properties of the wave modes, the wave amplitude vectors $\mathbf{Q}_{\mathtt{b}}^{(k)}$ and $\mathbf{Q}_{\mathtt{b}}^{\star(k)}$ can

be expressed as [7]:

$$\mathbf{Q}_{\mathtt{b}}^{(k)} = (\mathbf{\Phi}^{\star T}\mathbf{J}\mathbf{\Phi})^{-1}\mathbf{\Phi}^{\star T}\mathbf{J}\mathbf{b}^{(k)} \qquad , \qquad \mathbf{Q}_{\mathtt{b}}^{\star(k)} = (\mathbf{\Phi}^{T}\mathbf{J}\mathbf{\Phi}^{\star})^{-1}\mathbf{\Phi}^{T}\mathbf{J}\mathbf{b}^{(k)}, \tag{16}$$

where $\mathbf{\Phi}^{\star T}\mathbf{J}\mathbf{\Phi}$ and $\mathbf{\Phi}^{T}\mathbf{J}\mathbf{\Phi}^{\star}$ are diagonal matrices with the property that $(\mathbf{\Phi}^{T}\mathbf{J}\mathbf{\Phi}^{\star})^{T} = \mathbf{\Phi}^{T}\mathbf{J}\mathbf{\Phi}^{\star} = -\mathbf{\Phi}^{\star T}\mathbf{J}\mathbf{\Phi}$. To determine the displacement and force vectors at the substructure interfaces, the wave amplitude vectors $\mathbf{Q}^{(k)}$ and $\mathbf{Q}^{\star(k)}$ in Eq. (14) must be computed. For this purpose, the following methodology is used:

(i) Express the wave amplitude vectors $\mathbf{Q}^{(k)}$ and $\mathbf{Q}^{\star(k)}$ at any substructure interface (k) $(k = 1, \ldots, N)$ from the wave amplitudes vectors $\mathbf{Q} = \mathbf{Q}^{(1)}$ and $\mathbf{Q}^{\star} = \mathbf{Q}^{\star(N)}$ at the left and right sides Γ_+ and Γ_- (respectively) of the substructure enclosed between the interfaces (N) and (1), see Fig. 2.

(ii) Compute $\mathbf{Q}$ and $\mathbf{Q}^{\star}$ by considering the dynamic equation of this substructure.

The main steps of the methodology are given here. First, introducing the wave expansions (14) and (15) into Eq. (9) and using the orthogonality properties of the wave modes yields:

$$\mathbf{Q}^{(k+1)} = \boldsymbol{\mu}\mathbf{Q}^{(k)} + \mathbf{Q}_{\mathtt{b}}^{(k)}. \tag{17}$$

Eq. (17) provides a recurrence relation between two consecutive substructures. This yields:

$$\mathbf{Q}^{(k)} = \boldsymbol{\mu}^{k-1}\mathbf{Q} + \sum_{p=1}^{k-1} \boldsymbol{\mu}^{k-1-p}\mathbf{Q}_{\mathtt{b}}^{(p)} \qquad \text{for } k = 2, \ldots, N, \tag{18}$$

where $\mathbf{Q} = \mathbf{Q}^{(1)}$ denotes the wave amplitude vector for the forward-going waves at the interface (1), see Fig. 2. In the same way, the following recurrence relation can be obtained:

$$\mathbf{Q}^{\star(k+1)} = \boldsymbol{\mu}^{\star}\mathbf{Q}^{\star(k)} + \mathbf{Q}_{\mathtt{b}}^{\star(k)}. \tag{19}$$

This yields (see [7] for the proof):

$$\mathbf{Q}^{\star(k)} = \boldsymbol{\mu}^{N-k}\mathbf{Q}^{\star} - \sum_{p=k}^{N-1} \boldsymbol{\mu}^{-k+1+p}\mathbf{Q}_{\mathtt{b}}^{\star(p)} \qquad \text{for } k = 1, \ldots, N-1. \tag{20}$$

with $\mathbf{Q}^{\star} = \mathbf{Q}^{\star(N)}$ the wave amplitude vector for the backward-going waves at the interface (N), see Fig. 2. Eqs. (18) and (20) mean that the wave amplitude vectors $\mathbf{Q}^{(k)}$ and $\mathbf{Q}^{\star(k)}$, at any substructure interface (k), can be expressed from the wave amplitude vectors $\mathbf{Q}$ and $\mathbf{Q}^{\star}$ for the forward- and backward-going waves at the left and right sides Γ_+ and Γ_- of the substructure enclosed between the interfaces (N) and (1). To compute $\mathbf{Q}$ and $\mathbf{Q}^{\star}$, the dynamic equation of this substructure is considered [5]. Hence, let us consider Eq. (2), i.e.,

$$\mathbf{D}^{*} \begin{bmatrix} \mathbf{q}_{\Gamma_-}^{(N)} \\ \mathbf{q}_{\Gamma_+}^{(1)} \end{bmatrix} = \begin{bmatrix} \mathbf{F}_{\Gamma_-}^{(N)} \\ \mathbf{F}_{\Gamma_+}^{(1)} \end{bmatrix} + \begin{bmatrix} \mathbf{F}_{\mathtt{I}}^{*(N)}|_{\Gamma_-} \\ \mathbf{F}_{\mathtt{I}}^{*(N)}|_{\Gamma_+} \end{bmatrix}. \tag{21}$$

By considering a wave mode expansion for the displacement and force vectors at the interfaces (N) and (1), see Eq. (14) together with Eqs. (18) and (20), this yields:

$$\mathbf{q}_{\Gamma_-}^{(N)} = \mathbf{\Phi}_{\mathtt{q}}\mathbf{Q}^{(N)} + \mathbf{\Phi}_{\mathtt{q}}^{\star}\mathbf{Q}^{\star(N)} = \mathbf{\Phi}_{\mathtt{q}} \left(\boldsymbol{\mu}^{N-1}\mathbf{Q} + \sum_{p=1}^{N-1} \boldsymbol{\mu}^{N-1-p}\mathbf{Q}_{\mathtt{b}}^{(p)} \right) + \mathbf{\Phi}_{\mathtt{q}}^{\star}\mathbf{Q}^{\star}, \tag{22}$$

$$\mathbf{q}_{\Gamma_+}^{(1)} = \mathbf{\Phi}_{\mathtt{q}}\mathbf{Q}^{(1)} + \mathbf{\Phi}_{\mathtt{q}}^{\star}\mathbf{Q}^{\star(1)} = \mathbf{\Phi}_{\mathtt{q}}\mathbf{Q} + \mathbf{\Phi}_{\mathtt{q}}^{\star} \left(\boldsymbol{\mu}^{N-1}\mathbf{Q}^{\star} - \sum_{p=1}^{N-1} \boldsymbol{\mu}^{p}\mathbf{Q}_{\mathtt{b}}^{\star(p)} \right), \tag{23}$$

and

$$\mathbf{F}_{\Gamma_-}^{(N)} = -\left(\mathbf{\Phi}_{\mathtt{F}}\mathbf{Q}^{(N)} + \mathbf{\Phi}_{\mathtt{F}}^{\star}\mathbf{Q}^{\star(N)}\right) = -\mathbf{\Phi}_{\mathtt{F}}\left(\boldsymbol{\mu}^{N-1}\mathbf{Q} + \sum_{p=1}^{N-1}\boldsymbol{\mu}^{N-1-p}\mathbf{Q}_{\mathtt{b}}^{(p)}\right) - \mathbf{\Phi}_{\mathtt{F}}^{\star}\mathbf{Q}^{\star}, \tag{24}$$

$$\mathbf{F}_{\Gamma_+}^{(1)} = \mathbf{\Phi}_{\mathtt{F}}\mathbf{Q}^{(1)} + \mathbf{\Phi}_{\mathtt{F}}^{\star}\mathbf{Q}^{\star(1)} = \mathbf{\Phi}_{\mathtt{F}}\mathbf{Q} + \mathbf{\Phi}_{\mathtt{F}}^{\star}\left(\boldsymbol{\mu}^{N-1}\mathbf{Q}^{\star} - \sum_{p=1}^{N-1}\boldsymbol{\mu}^{p}\mathbf{Q}_{\mathtt{b}}^{\star(p)}\right). \tag{25}$$

Then, Eq. (21) leads to:

$$\left(\mathbf{D}^*\begin{bmatrix}\mathbf{\Phi}_{\mathtt{q}}\boldsymbol{\mu}^{N-1} & \mathbf{\Phi}_{\mathtt{q}}^{\star} \\ \mathbf{\Phi}_{\mathtt{q}} & \mathbf{\Phi}_{\mathtt{q}}^{\star}\boldsymbol{\mu}^{N-1}\end{bmatrix} - \begin{bmatrix}-\mathbf{\Phi}_{\mathtt{F}}\boldsymbol{\mu}^{N-1} & -\mathbf{\Phi}_{\mathtt{F}}^{\star} \\ \mathbf{\Phi}_{\mathtt{F}} & \mathbf{\Phi}_{\mathtt{F}}^{\star}\boldsymbol{\mu}^{N-1}\end{bmatrix}\right)\begin{bmatrix}\mathbf{Q} \\ \mathbf{Q}^{\star}\end{bmatrix} \tag{26}$$

$$= \left(\mathbf{D}^*\mathbf{\Psi}_{\mathtt{qb}} - \mathbf{\Psi}_{\mathtt{Fb}}\right)\begin{bmatrix}\sum_{p=1}^{N-1}\boldsymbol{\mu}^{N-1-p}\mathbf{Q}_{\mathtt{b}}^{(p)} \\ \sum_{p=1}^{N-1}\boldsymbol{\mu}^{p}\mathbf{Q}_{\mathtt{b}}^{\star(p)}\end{bmatrix} + \begin{bmatrix}\mathbf{F}_{\mathtt{I}}^{*(N)}|_{\Gamma_-} \\ \mathbf{F}_{\mathtt{I}}^{*(N)}|_{\Gamma_+}\end{bmatrix},$$

where

$$\mathbf{\Psi}_{\mathtt{qb}} = \begin{bmatrix}-\mathbf{\Phi}_{\mathtt{q}} & \mathbf{0} \\ \mathbf{0} & \mathbf{\Phi}_{\mathtt{q}}^{\star}\end{bmatrix} \quad , \quad \mathbf{\Psi}_{\mathtt{Fb}} = \begin{bmatrix}\mathbf{\Phi}_{\mathtt{F}} & \mathbf{0} \\ \mathbf{0} & \mathbf{\Phi}_{\mathtt{F}}^{\star}\end{bmatrix}. \tag{27}$$

Eq. (26) represents a matrix equation of the form $\boldsymbol{\mathcal{A}}\boldsymbol{\mathcal{Q}} = \boldsymbol{\mathcal{G}}$ with $\boldsymbol{\mathcal{Q}} = [\mathbf{Q}^T\mathbf{Q}^{\star T}]^T$ and $\boldsymbol{\mathcal{A}}$ a $2n \times 2n$ matrix. Solving this equation yields the wave amplitudes vectors $\mathbf{Q}$ and $\mathbf{Q}^{\star}$. The wave amplitude vectors $\mathbf{Q}^{(k)}$ and $\mathbf{Q}^{\star(k)}$ at any interface (k) ($k = 1, \ldots, N$) can be easily retrieved from Eqs. (18) and (20). Also, the displacement and force vectors at the interface (k) can be retrieved Eq. (14). Finally, the displacement vectors for the internal nodes of the substructures can be retrieved from Eq. (1), by considering a substructure enclosed between two interfaces (k) and $(k+1)$:

$$\mathbf{q}_{\mathtt{I}}^{(k)} = \mathbf{D}_{\mathtt{II}}^{-1}\left(\mathbf{F}_{\mathtt{I}}^{(k)} - \mathbf{D}_{\mathtt{I}\Gamma_-}\mathbf{q}_{\Gamma_-}^{(k)} - \mathbf{D}_{\mathtt{I}\Gamma_+}\mathbf{q}_{\Gamma_+}^{(k+1)}\right). \tag{28}$$

2.4 Engine order excitation

Often in industrial situations, the external forces applied to the substructures result from an engine order excitation, i.e.,

$$\mathbf{F}_{\mathtt{I}}^{(k)} = \mathbf{F}_{\mathtt{I}}^{(N)}e^{-\mathtt{i}k\frac{2\pi\mathrm{EO}}{N}} \qquad \text{for } k = 1, \ldots, N-1, \tag{29}$$

with $\mathbf{F}_{\mathtt{I}}^{(N)}$ the known vector of external forces applied to the substructure enclosed between the interfaces (N) and (1), and EO the engine order (EO $= 0, 1, 2, \ldots$). Within this framework, the wave amplitude vectors for the external loads, Eq. (16), become $\mathbf{Q}_{\mathtt{b}}^{(k)} = e^{-\mathtt{i}k\frac{2\pi\mathrm{EO}}{N}}\mathbf{Q}_{\mathtt{b}}^{(N)}$ and $\mathbf{Q}_{\mathtt{b}}^{\star(k)} = e^{-\mathtt{i}k\frac{2\pi\mathrm{EO}}{N}}\mathbf{Q}_{\mathtt{b}}^{\star(N)}$. Then, the vector sums on the right-hand side of Eq. (26) simplify to:

$$\sum_{p=1}^{N-1}\boldsymbol{\mu}^{N-1-p}\mathbf{Q}_{\mathtt{b}}^{(p)} = \left(\sum_{p=1}^{N-1}\boldsymbol{\mu}^{N-1-p}e^{-\mathtt{i}k\frac{2\pi\mathrm{EO}}{N}}\right)\mathbf{Q}_{\mathtt{b}}^{(N)}, \sum_{p=1}^{N-1}\boldsymbol{\mu}^{p}\mathbf{Q}_{\mathtt{b}}^{\star(p)} = \left(\sum_{p=1}^{N-1}\boldsymbol{\mu}^{p}e^{-\mathtt{i}k\frac{2\pi\mathrm{EO}}{N}}\right)\mathbf{Q}_{\mathtt{b}}^{\star(N)}. \tag{30}$$

2.5 Mistuned bladed disks

The WFE strategy to model bladed disks with one or two perturbed substructures (see Fig. 3) is detailed hereafter. Note that the proposed strategy is general as it could be easily extended to include more perturbed substructures. Perturbed substructures can result from parametric changes, e.g., modifications of the material properties or variations of the substructure shape (mesh parameters). To carry out the modeling of mistuned bladed disks, the following relations that concern the wave amplitude vectors for a substructure enclosed between two interfaces (k_1) and $(k_1 + 1)$ and a substructure enclosed between two interfaces (k_2) and

(k_2+1) with $k_2 > k_1$ are proposed:

$$\mathbf{Q}^{\star(k_1+1)} = \boldsymbol{\mu}^{k_2-k_1-1}\mathbf{Q}^{\star(k_2)} - \sum_{p=k_1+1}^{k_2-1} \boldsymbol{\mu}^{-k_1+p}\mathbf{Q}_{\mathtt{b}}^{\star(p)}, \tag{31}$$

$$\mathbf{Q}^{(k_2)} = \boldsymbol{\mu}^{k_2-k_1-1}\mathbf{Q}^{(k_1+1)} + \sum_{p=k_1+1}^{k_2-1} \boldsymbol{\mu}^{k_2-1-p}\mathbf{Q}_{\mathtt{b}}^{(p)}. \tag{32}$$

Eqs. (31) and (32) come from Eqs. (17) and (19) and constitute a general framework for expressing the wave amplitude vectors at arbitrary interfaces (k_1+1) and (k_2).

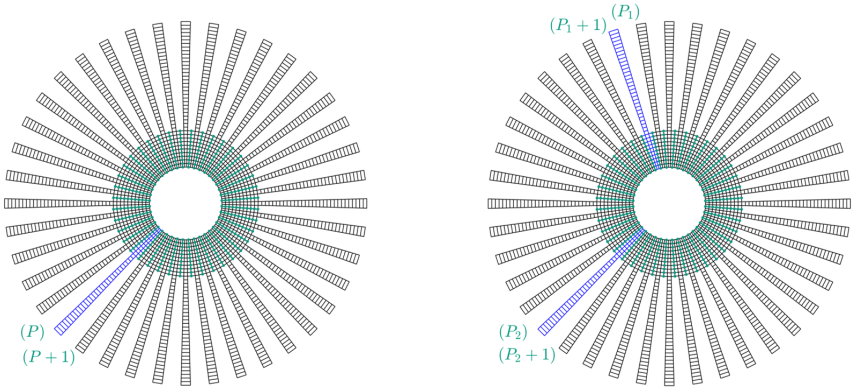

Figure 3: Mistuned bladed disk (simple 2D case): (left) one perturbed substructure (blue color) enclosed between two interfaces (P) and $(P+1)$; (right) two perturbed substructures (blue color) enclosed between two interfaces (P_1) and (P_1+1) and between two interfaces (P_2) and (P_2+1), respectively.

2.5.1 One perturbed substructure

A periodic structure with a perturbed substructure, whose condensed dynamic stiffness matrix is $\mathbf{D}_P^* \neq \mathbf{D}^*$, enclosed between two consecutive interfaces (P) and $(P+1)$ is shown in Fig. (3). A wave-based modeling can be proposed in a similar way as in Sec. 2.3. Indeed in this case, the strategy simply consists in expressing the displacement and force vectors at the boundaries of the perturbed substructure as in Eqs. (22)-(25):

$$\mathbf{q}_{\Gamma_-}^{(P)} = \boldsymbol{\Phi}_{\mathtt{q}}\mathbf{Q}^{(P)} + \boldsymbol{\Phi}_{\mathtt{q}}^{\star}\mathbf{Q}^{\star(P)} \quad , \quad \mathbf{q}_{\Gamma_+}^{(P+1)} = \boldsymbol{\Phi}_{\mathtt{q}}\mathbf{Q}^{(P+1)} + \boldsymbol{\Phi}_{\mathtt{q}}^{\star}\mathbf{Q}^{\star(P+1)}, \tag{33}$$

$$\mathbf{F}_{\Gamma_-}^{(P)} = -\left(\boldsymbol{\Phi}_{\mathtt{F}}\mathbf{Q}^{(P)} + \boldsymbol{\Phi}_{\mathtt{F}}^{\star}\mathbf{Q}^{\star(P)}\right) \quad , \quad \mathbf{F}_{\Gamma_+}^{(P+1)} = \boldsymbol{\Phi}_{\mathtt{F}}\mathbf{Q}^{(P+1)} + \boldsymbol{\Phi}_{\mathtt{F}}^{\star}\mathbf{Q}^{\star(P+1)}. \tag{34}$$

where $\mathbf{Q}^{(P)}$, $\mathbf{Q}^{\star(P)}$, $\mathbf{Q}^{(P+1)}$ and $\mathbf{Q}^{\star(P+1)}$ are wave amplitude vectors for the interfaces (P) and $(P+1)$. By considering Eqs. (31) and (32) with $k_1 = P$ and $k_2 = P+N$ (i.e., $k_2 = k_1$ modulo N), and the dynamic equation of the perturbed substructure, Eq. (26) with $\mathbf{D}^* \to \mathbf{D}_P^*$, one obtains:

$$\begin{aligned}\left(\mathbf{D}_P^* \begin{bmatrix} \boldsymbol{\Phi}_{\mathtt{q}}\boldsymbol{\mu}^{N-1} & \boldsymbol{\Phi}_{\mathtt{q}}^{\star} \\ \boldsymbol{\Phi}_{\mathtt{q}} & \boldsymbol{\Phi}_{\mathtt{q}}^{\star}\boldsymbol{\mu}^{N-1} \end{bmatrix} - \begin{bmatrix} -\boldsymbol{\Phi}_{\mathtt{F}}\boldsymbol{\mu}^{N-1} & -\boldsymbol{\Phi}_{\mathtt{F}}^{\star} \\ \boldsymbol{\Phi}_{\mathtt{F}} & \boldsymbol{\Phi}_{\mathtt{F}}^{\star}\boldsymbol{\mu}^{N-1} \end{bmatrix}\right) \begin{bmatrix} \mathbf{Q}^{(P+1)} \\ \mathbf{Q}^{\star(P)} \end{bmatrix} \\ = \left(\mathbf{D}_P^*\boldsymbol{\Psi}_{\mathtt{qb}} - \boldsymbol{\Psi}_{\mathtt{Fb}}\right) \begin{bmatrix} \sum_{p=P+1}^{N+P-1} \boldsymbol{\mu}^{N+P-1-p}\mathbf{Q}_{\mathtt{b}}^{(p)} \\ \sum_{p=P+1}^{N+P-1} \boldsymbol{\mu}^{-P+p}\mathbf{Q}_{\mathtt{b}}^{\star(p)} \end{bmatrix} + \begin{bmatrix} \mathbf{F}_{\mathtt{I}}^{*(P)}|_{\Gamma_-} \\ \mathbf{F}_{\mathtt{I}}^{*(P)}|_{\Gamma_+} \end{bmatrix}.\end{aligned} \tag{35}$$

Solving Eq. (35) yields the wave amplitude vectors $\mathbf{Q}^{(P+1)}$ and $\mathbf{Q}^{\star(P)}$. The determination of the wave amplitude vectors $\mathbf{Q}^{(k)}$ and $\mathbf{Q}^{\star(k)}$ at any interface (k) follows from Eqs. (31) and (32).

2.5.2 Two perturbed substructures

A periodic structure with two perturbed substructures with condensed dynamic stiffness matrices $\mathbf{D}^*_{P_1} \neq \mathbf{D}^*$ and $\mathbf{D}^*_{P_2} \neq \mathbf{D}^*$ enclosed, respectively, between two interfaces (P_1) and (P_1+1) and between two interfaces (P_2) and (P_2+1) is shown in Fig. 2. In the case of consecutive perturbed substructures (i.e., when $P_2 = P_1 + 1$), the analysis is straightforward and quite similar to the previous case. In short, this consists in expressing the dynamic equation of the assembly made of these substructures, and expressing wave amplitude vectors at the boundaries Γ_- and Γ_+ in the same way as in the previous example, see Eq. (35). For non-consecutive perturbed substructures, the strategy consists in expressing the displacement and force vectors at the boundaries of the perturbed substructures in wave shape bases in the same way as in Eqs. (33)-(34). Then, by considering the dynamic equations of the perturbed substructures and Eqs. (31) and (32), the following wave-based matrix equations can be derived:

$$\begin{aligned}
&\left(\mathbf{D}^*_{P_1}\begin{bmatrix}\boldsymbol{\Phi}_{\mathtt{q}}\boldsymbol{\mu}^{N+P_1-P_2-1} & \boldsymbol{\Phi}^\star_{\mathtt{q}} & \mathbf{0} & \mathbf{0}\\ \mathbf{0} & \mathbf{0} & \boldsymbol{\Phi}_{\mathtt{q}} & \boldsymbol{\Phi}^\star_{\mathtt{q}}\boldsymbol{\mu}^{P_2-P_1-1}\end{bmatrix}\right. \\
&\left.-\begin{bmatrix}-\boldsymbol{\Phi}_{\mathtt{F}}\boldsymbol{\mu}^{N+P_1-P_2-1} & -\boldsymbol{\Phi}^\star_{\mathtt{F}} & \mathbf{0} & \mathbf{0}\\ \mathbf{0} & \mathbf{0} & \boldsymbol{\Phi}_{\mathtt{F}} & \boldsymbol{\Phi}^\star_{\mathtt{F}}\boldsymbol{\mu}^{P_2-P_1-1}\end{bmatrix}\right)\begin{bmatrix}\mathbf{Q}^{(P_2+1)}\\ \mathbf{Q}^{\star(P_1)}\\ \mathbf{Q}^{(P_1+1)}\\ \mathbf{Q}^{\star(P_2)}\end{bmatrix} \\
&= \left(\mathbf{D}^*_{P_1}\boldsymbol{\Psi}_{\mathtt{qb}} - \boldsymbol{\Psi}_{\mathtt{Fb}}\right)\begin{bmatrix}\sum_{p=P_2+1}^{N+P_1-1}\boldsymbol{\mu}^{N+P_1-1-p}\mathbf{Q}^{(p)}_{\mathtt{b}}\\ \sum_{p=P_1}^{P_2-1}\boldsymbol{\mu}^{-P_1+p}\mathbf{Q}^{\star(p)}_{\mathtt{b}}\end{bmatrix} + \begin{bmatrix}\mathbf{F}^{*(P_1)}_{\mathtt{I}}|_{\Gamma_-}\\ \mathbf{F}^{*(P_1)}_{\mathtt{I}}|_{\Gamma_+}\end{bmatrix},
\end{aligned} \tag{36}$$

and

$$\begin{aligned}
&\left(\mathbf{D}^*_{P_2}\begin{bmatrix}\mathbf{0} & \mathbf{0} & \boldsymbol{\Phi}_{\mathtt{q}}\boldsymbol{\mu}^{P_2-P_1-1} & \boldsymbol{\Phi}^\star_{\mathtt{q}}\\ \boldsymbol{\Phi}_{\mathtt{q}} & \boldsymbol{\Phi}^\star_{\mathtt{q}}\boldsymbol{\mu}^{N+P_1-P_2-1} & \mathbf{0} & \mathbf{0}\end{bmatrix}\right. \\
&\left.-\begin{bmatrix}\mathbf{0} & \mathbf{0} & -\boldsymbol{\Phi}_{\mathtt{F}}\boldsymbol{\mu}^{P_2-P_1-1} & -\boldsymbol{\Phi}^\star_{\mathtt{F}}\\ \boldsymbol{\Phi}_{\mathtt{F}} & \boldsymbol{\Phi}^\star_{\mathtt{F}}\boldsymbol{\mu}^{N+P_1-P_2-1} & \mathbf{0} & \mathbf{0}\end{bmatrix}\right)\begin{bmatrix}\mathbf{Q}^{(P_2+1)}\\ \mathbf{Q}^{\star(P_1)}\\ \mathbf{Q}^{(P_1+1)}\\ \mathbf{Q}^{\star(P_2)}\end{bmatrix} \\
&= \left(\mathbf{D}^*_{P_2}\boldsymbol{\Psi}_{\mathtt{qb}} - \boldsymbol{\Psi}_{\mathtt{Fb}}\right)\begin{bmatrix}\sum_{p=P_1+1}^{P_2-1}\boldsymbol{\mu}^{P_2-1-p}\mathbf{Q}^{(p)}_{\mathtt{b}}\\ \sum_{p=P_2+1}^{N+P_1-1}\boldsymbol{\mu}^{-P_2+p}\mathbf{Q}^{\star(p)}_{\mathtt{b}}\end{bmatrix} + \begin{bmatrix}\mathbf{F}^{*(P_2)}_{\mathtt{I}}|_{\Gamma_-}\\ \mathbf{F}^{*(P_2)}_{\mathtt{I}}|_{\Gamma_+}\end{bmatrix}.
\end{aligned} \tag{37}$$

Eqs. (36) and (37) can be combined so as to express a matrix equation of the form $\boldsymbol{\mathcal{A}}\boldsymbol{\mathcal{Q}} = \boldsymbol{\mathcal{G}}$, where $\boldsymbol{\mathcal{A}}$ represents a $4n \times 4n$ matrix that results from stacking the terms inside the brackets on the left-hand side of Eqs. (36) and (37), and $\boldsymbol{\mathcal{Q}}$ is a vector with components $\mathbf{Q}^{(P_2+1)}$, $\mathbf{Q}^{\star(P_1)}$, $\mathbf{Q}^{(P_1+1)}$, $\mathbf{Q}^{\star(P_2)}$.

3 Model reduction

In industrial situations, 3D substructures are usually involved whose FE models are likely to contain many internal and interface DOFs. In this case, model reduction techniques are required to improve the efficiency of the WFE method. First, to quickly compute the condensed dynamic stiffness matrix of the substructures $\mathbf{D}^*$ as well as the vector $\mathbf{F}^{*(N)}_{\mathtt{I}}$ in Eq. (2), a CB reduction of the number of internal DOFs is proposed [9]. For instance, the CB strategy to compute $\mathbf{D}^*$ consists in:

1. Partitioning a substructure into boundary DOFs (`B`), including the interface and excitation DOFs, and internal DOFs (`I`) which are free from excitation.

2. Approximating the displacement vector for the internal DOFs using static modes (matrix $\mathbf{X}_{\mathtt{st}}$) and a reduced number $M_{\mathtt{I}}$ of fixed interface modes (matrix $\widetilde{\mathbf{X}}$), i.e., $\mathbf{q}_{\mathtt{I}} \approx \mathbf{X}_{\mathtt{st}}\mathbf{q}_{\mathtt{B}} + \widetilde{\mathbf{X}}\widetilde{\boldsymbol{\alpha}}$ where $\widetilde{\boldsymbol{\alpha}}$ denotes the vector of generalized coordinates for the fixed interface modes.

3. Expressing the transformation matrix $\widetilde{\mathbf{T}}$ of the substructure in terms of static modes and fixed interface modes, and expressing the reduced substructure matrices as $\widetilde{\mathbf{M}} = \widetilde{\mathbf{T}}^T\mathbf{M}\widetilde{\mathbf{T}}$, $\widetilde{\mathbf{C}} = \widetilde{\mathbf{T}}^T\mathbf{C}\widetilde{\mathbf{T}}$ and $\widetilde{\mathbf{K}} = \widetilde{\mathbf{T}}^T\mathbf{K}\widetilde{\mathbf{T}}$.

4. Condensing the DOFs associated with the fixed interface modes onto the boundary DOFs, i.e., $\mathbf{D}^* = \widetilde{\mathbf{D}}_{\mathtt{BB}} - \widetilde{\mathbf{D}}_{\mathtt{B}\alpha}\widetilde{\mathbf{D}}_{\alpha\alpha}^{-1}\widetilde{\mathbf{D}}_{\alpha\mathtt{B}}$.

5. Condensing the excitation DOFs onto the interface DOFs (in the same way as in the previous step). The resulting condensed DSM will be also denoted by $\mathbf{D}^*$.

Next, to speed up the computation of the wave modes, an interface reduction is proposed (see hereafter).

3.1 Interface reduction

Let $\widetilde{\mathbf{M}}_{\Gamma\Gamma}$ and $\widetilde{\mathbf{K}}_{\Gamma\Gamma}$ denote the block components of the reduced mass and stiffness matrices of a substructure $\widetilde{\mathbf{M}}$ and $\widetilde{\mathbf{K}}$ (CB reduction) which are associated with the interface DOFs (Γ_- and Γ_+). Then define the boundary modes of the substructure as the eigenvectors $\boldsymbol{\chi}_j$ of the matrix pencil $(\widetilde{\mathbf{K}}_{\Gamma\Gamma}, \widetilde{\mathbf{M}}_{\Gamma\Gamma})$. A reduced matrix of boundary modes can be expressed as $\widetilde{\mathbf{X}}_\Gamma = [\boldsymbol{\chi}_1 \cdots \boldsymbol{\chi}_{m_\Gamma}]$ with $m_\Gamma \ll 2n$ a number of low-order modes (i.e., associated with m_Γ smallest eigenvalues λ_j). The boundary modes involve the DOFs on Γ_- and Γ_+ and, therefore, the matrix $\widetilde{\mathbf{X}}_\Gamma$ has to be expressed as:

$$\widetilde{\mathbf{X}}_\Gamma = \begin{bmatrix} \widetilde{\mathbf{X}}_{\Gamma_-} \\ \widetilde{\mathbf{X}}_{\Gamma_+} \end{bmatrix}. \tag{38}$$

A common reduced matrix of boundary modes for Γ_- and Γ_+ can be obtained from a singular value decomposition of $[\widetilde{\mathbf{X}}_{\Gamma_-}\ \widetilde{\mathbf{X}}_{\Gamma_+}]$, i.e. [11]:

$$[\widetilde{\mathbf{X}}_{\Gamma_-}\ \widetilde{\mathbf{X}}_{\Gamma_+}] = \mathbf{U}_\Gamma \boldsymbol{\Sigma}_\Gamma \mathbf{V}_\Gamma^T, \tag{39}$$

with $\boldsymbol{\Sigma}_\Gamma$ the matrix of singular values, and $\mathbf{U}_\Gamma$ and $\mathbf{V}_\Gamma$ the related orthogonal matrices of left and right singular vectors (respectively). Especially the matrix $\mathbf{U}_\Gamma$ contains $m = 2m_\Gamma$ orthogonal column vectors with the property that they span the same space as the column vectors contained in $\widetilde{\mathbf{X}}_{\Gamma_-}$ and $\widetilde{\mathbf{X}}_{\Gamma_+}$. Therefore the following approximation for the interface DOFs can be proposed:

$$\mathbf{q}_{\Gamma_-} \approx \widetilde{\mathbf{q}}_{\Gamma_-} = \mathbf{U}_\Gamma\, \widetilde{\boldsymbol{\alpha}}_{\Gamma_-} \qquad , \qquad \mathbf{q}_{\Gamma_+} \approx \widetilde{\mathbf{q}}_{\Gamma_+} = \mathbf{U}_\Gamma\, \widetilde{\boldsymbol{\alpha}}_{\Gamma_+}, \tag{40}$$

where $\widetilde{\boldsymbol{\alpha}}_{\Gamma_-}$ and $\widetilde{\boldsymbol{\alpha}}_{\Gamma_+}$ are $m \times 1$ vectors of generalized coordinates. Then, the following reduced condensed dynamic stiffness matrix of a substructure can be proposed:

$$\widetilde{\mathbf{D}}^* = \begin{bmatrix} \widetilde{\mathbf{D}}^*_{\Gamma_-\Gamma_-} & \widetilde{\mathbf{D}}^*_{\Gamma_-\Gamma_+} \\ \widetilde{\mathbf{D}}^*_{\Gamma_+\Gamma_-} & \widetilde{\mathbf{D}}^*_{\Gamma_+\Gamma_+} \end{bmatrix} = \begin{bmatrix} \mathbf{U}_\Gamma & \mathbf{0} \\ \mathbf{0} & \mathbf{U}_\Gamma \end{bmatrix}^T \begin{bmatrix} \mathbf{D}^*_{\Gamma_-\Gamma_-} & \mathbf{D}^*_{\Gamma_-\Gamma_+} \\ \mathbf{D}^*_{\Gamma_+\Gamma_-} & \mathbf{D}^*_{\Gamma_+\Gamma_+} \end{bmatrix} \begin{bmatrix} \mathbf{U}_\Gamma & \mathbf{0} \\ \mathbf{0} & \mathbf{U}_\Gamma \end{bmatrix}. \tag{41}$$

Also, since the matrix $\mathbf{U}_\Gamma$ is orthogonal, it can be proven that the force vectors $\mathbf{F}_{\Gamma_-}$ and $\mathbf{F}_{\Gamma_+}$ can be approximated as:

$$\mathbf{F}_{\Gamma_-} \approx \widetilde{\mathbf{F}}_{\Gamma_-} = \mathbf{U}_\Gamma\, \widetilde{\boldsymbol{\beta}}_{\Gamma_-} \qquad , \qquad \mathbf{F}_{\Gamma_+} \approx \widetilde{\mathbf{F}}_{\Gamma_+} = \mathbf{U}_\Gamma\, \widetilde{\boldsymbol{\beta}}_{\Gamma_+}, \tag{42}$$

with $\widetilde{\boldsymbol{\beta}}_{\Gamma_-}$ and $\widetilde{\boldsymbol{\beta}}_{\Gamma_+}$ $m \times 1$ vectors of generalized coordinates. With this reduction technique, a transfer matrix $\widetilde{\mathbf{S}}$ of small size $2m \times 2m$ with $m \ll n$ can be established like in Eq. (7). Then the computation of the wave modes can be drastically sped up.

3.2 Error indicator

To assess the error induced by the model reduction technique, a force balance at the interfaces between the substructures can be considered. For instance, let us consider the substructure enclosed between the interfaces (N) and (1) as shown in Fig. 2, and let us assume for the sake of simplicity that this substructure as well as the two adjacent ones connected on Γ_- and Γ_+ are unperturbed, i.e., that these three substructures share the same condensed dynamic stiffness matrix $\mathbf{D}^*$. From Eq. (2), the boundary forces for the substructure enclosed between the interfaces (N) and (1) are expressed as:

$$\widetilde{\boldsymbol{\mathcal{F}}}_\Gamma = \begin{bmatrix} \widetilde{\boldsymbol{\mathcal{F}}}_{\Gamma_-}^{(N)} \\ \widetilde{\boldsymbol{\mathcal{F}}}_{\Gamma_+}^{(1)} \end{bmatrix} = \mathbf{D}^* \begin{bmatrix} \widetilde{\mathbf{q}}_{\Gamma_-}^{(N)} \\ \widetilde{\mathbf{q}}_{\Gamma_+}^{(1)} \end{bmatrix} - \mathbf{F}_{\mathtt{I}}^{*(N)}, \tag{43}$$

where $\mathbf{D}^*$ denotes the $2n \times 2n$ unreduced condensed dynamic stiffness matrix which results from Eq. (3) and the CB method. Here, $\widetilde{\mathbf{q}}_{\Gamma_-}^{(N)}$ and $\widetilde{\mathbf{q}}_{\Gamma_+}^{(1)}$ are the displacement vectors that result from model reduction, i.e., these vectors are expressed as:

$$\widetilde{\mathbf{q}}_{\Gamma_-}^{(N)} = \mathbf{U}_\Gamma \, \widetilde{\boldsymbol{\alpha}}_{\Gamma_-}^{(N)} = \mathbf{U}_\Gamma \left(\widetilde{\boldsymbol{\Phi}}_{\mathtt{q}} \widetilde{\mathbf{Q}}^{(N)} + \widetilde{\boldsymbol{\Phi}}_{\mathtt{q}}^{\star} \widetilde{\mathbf{Q}}^{\star(N)} \right) \ , \ \widetilde{\mathbf{q}}_{\Gamma_+}^{(1)} = \mathbf{U}_\Gamma \, \widetilde{\boldsymbol{\alpha}}_{\Gamma_+}^{(1)} = \mathbf{U}_\Gamma \left(\widetilde{\boldsymbol{\Phi}}_{\mathtt{q}} \widetilde{\mathbf{Q}}^{(1)} + \widetilde{\boldsymbol{\Phi}}_{\mathtt{q}}^{\star} \widetilde{\mathbf{Q}}^{\star(1)} \right). \tag{44}$$

In Eq. (43), $\widetilde{\boldsymbol{\mathcal{F}}}_{\Gamma_-}^{(N)}$ and $\widetilde{\boldsymbol{\mathcal{F}}}_{\Gamma_+}^{(1)}$ denote the interface forces which are computed from the dynamic equilibrium equation of the substructure when the displacement vectors are approximated as in Eq. (44). It should be pointed out that these force vectors are likely to differ from the reduced force vectors $\widetilde{\mathbf{F}}$ that would result from considering a wave expansion like in Eq. (14). On the other hand, the interfaces forces for the adjacent substructures can be expressed as:

$$\begin{bmatrix} \widehat{\boldsymbol{\mathcal{F}}}_{\Gamma_-}^{(N-1)} \\ \widehat{\boldsymbol{\mathcal{F}}}_{\Gamma_+}^{(N)} \end{bmatrix} = \mathbf{D}^* \begin{bmatrix} \widetilde{\mathbf{q}}_{\Gamma_-}^{(N-1)} \\ \widetilde{\mathbf{q}}_{\Gamma_+}^{(N)} \end{bmatrix} - \mathbf{F}_{\mathtt{I}}^{*(N-1)} \quad , \quad \begin{bmatrix} \widehat{\boldsymbol{\mathcal{F}}}_{\Gamma_-}^{(1)} \\ \widehat{\boldsymbol{\mathcal{F}}}_{\Gamma_+}^{(2)} \end{bmatrix} = \mathbf{D}^* \begin{bmatrix} \widetilde{\mathbf{q}}_{\Gamma_-}^{(1)} \\ \widetilde{\mathbf{q}}_{\Gamma_+}^{(2)} \end{bmatrix} - \mathbf{F}_{\mathtt{I}}^{*(1)}, \tag{45}$$

with $\widetilde{\mathbf{q}}_{\Gamma_+}^{(N)} = \widetilde{\mathbf{q}}_{\Gamma_-}^{(N)}$, $\widetilde{\mathbf{q}}_{\Gamma_-}^{(1)} = \widetilde{\mathbf{q}}_{\Gamma_+}^{(1)}$, $\widetilde{\mathbf{q}}_{\Gamma_-}^{(N-1)} = \mathbf{U}_\Gamma \, \widetilde{\boldsymbol{\alpha}}_{\Gamma_-}^{(N-1)}$ and $\widetilde{\mathbf{q}}_{\Gamma_+}^{(2)} = \mathbf{U}_\Gamma \, \widetilde{\boldsymbol{\alpha}}_{\Gamma_+}^{(2)}$. In Eq. (45), the vectors of coupling forces between the substructure enclosed between the interfaces (N) and (1) and the adjacent substructures are $\widehat{\boldsymbol{\mathcal{F}}}_{\Gamma_+}^{(N)}$ and $\widehat{\boldsymbol{\mathcal{F}}}_{\Gamma_-}^{(1)}$. In this sense, the following vector of interface forces can be defined:

$$\widehat{\boldsymbol{\mathcal{F}}}_\Gamma = \begin{bmatrix} \widehat{\boldsymbol{\mathcal{F}}}_{\Gamma_+}^{(N)} \\ \widehat{\boldsymbol{\mathcal{F}}}_{\Gamma_-}^{(1)} \end{bmatrix}. \tag{46}$$

By comparing the vectors of interface forces $\widehat{\boldsymbol{\mathcal{F}}}_\Gamma$ and $\widetilde{\boldsymbol{\mathcal{F}}}_\Gamma$ obtained from Eqs. (46) and (43) in the sense of a force balance — i.e., $\widehat{\boldsymbol{\mathcal{F}}}_\Gamma + \widetilde{\boldsymbol{\mathcal{F}}}_\Gamma$ —, an error indicator can be formulated. Here, $\widehat{\boldsymbol{\mathcal{F}}}_\Gamma + \widetilde{\boldsymbol{\mathcal{F}}}_\Gamma$ represents the residual force vector that arises from model reduction. The related error in displacement can be expressed as $(\mathbf{D}^*)^{-1}(\widehat{\boldsymbol{\mathcal{F}}}_\Gamma + \widetilde{\boldsymbol{\mathcal{F}}}_\Gamma)$. Then the following error indicator can be proposed:

$$\mathcal{E} = \frac{\|(\mathbf{D}^*)^{-1}(\widehat{\boldsymbol{\mathcal{F}}}_\Gamma + \widetilde{\boldsymbol{\mathcal{F}}}_\Gamma)\|_2}{\|(\mathbf{D}^*)^{-1}\widetilde{\boldsymbol{\mathcal{F}}}_\Gamma\|_2}. \tag{47}$$

4 Numerical results

The dynamic behavior of an industrial bladed disk with $N = 24$ sectors (3D substructures) is investigated where, in the present case, the tips of the blades are subjected to an engine order excitation with engine order EO $= 3$ (point forces of magnitudes 1 N $\times \, e^{-\mathtt{i}k\frac{2\pi \mathrm{EO}}{N}}$ in the circumferential direction). The relevant characteristics of the structure are: inner and outer radii of the disk $R_{\mathtt{i}}^{\mathtt{disk}} = 50$ mm and $R_{\mathtt{e}}^{\mathtt{disk}} = 212$ mm (respectively), radius of the tips of the blades $R^{\mathtt{tip}} = 280$ mm, density $\rho = 7800$ kg/m^3, Young's modulus

$E = 200$ GPa and Poisson's ratio $\nu = 0.25$. The inner surface of the disk is assumed to be clamped. The FE meshes of (i) the whole structure and (ii) a substructure are shown in Fig. 4. The FE models are built from 20-node quadratic hexahedrons, leading to $192,096$ DOFs for the whole structure and 8730 DOFs for the substructures including $n = 726$ DOFs on each interface Γ_- or Γ_+. Rayleigh-type damping is assumed where the damping matrices of the structure and the substructures are given by $\mathbf{C} = a\mathbf{M} + b\mathbf{K}$ with $a = 10^{-2}$ s^{-1} and $b = 10^{-8}$ s.

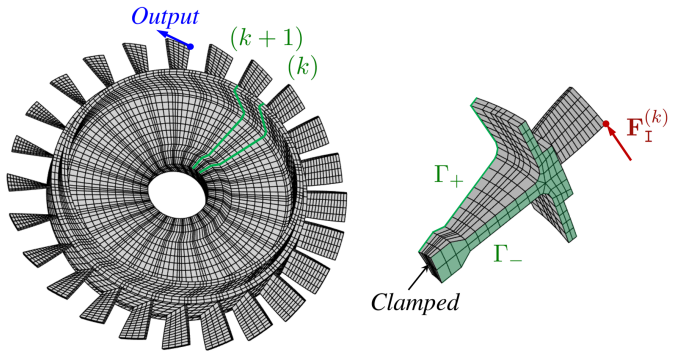

Figure 4: (Left) Bladed disk with 3D substructures ($N = 24$ substructures) subjected to an engine order excitation $\mathbf{F}_{\mathtt{I}}^{(k)} = 1\text{ N} \times e^{-\mathtt{i}k\frac{2\pi\mathrm{EO}}{N}}$; output point represents the absolute value of the tangential acceleration at the tip of the substructure enclosed between the interfaces (N) and (1). (Right) FE mesh of a substructure (inner boundary is clamped).

The dynamic behavior of the tuned disk (periodic structure) is predicted for frequency $f = \omega/2\pi$ up to 5000 Hz (frequency step $\Delta f = 0.5$ Hz). Also, the dynamic behavior of mistuned disks is discussed, where the following cases are considered:

1. A structure with a perturbed substructure referred to as mistuned bladed disk 1. In this case, the Young's modulus and, therefore, the stiffness matrix of the (only) blade of the substructure enclosed between the interfaces (15) and (16) are changed as $E_P^{\mathtt{blade}} = E^{\mathtt{blade}}(1 + 0.015)$ and $\mathbf{K}_P^{\mathtt{blade}} = \mathbf{K}^{\mathtt{blade}}(1 + 0.015)$.

2. A structure with two perturbed substructures referred to as mistuned bladed disk 2. In this case, the Young's moduli (resp. stiffness matrices) of the blades of the substructures enclosed between the interfaces (2) and (3) and between the interfaces (15) and (16) are changed as $E_{P_1}^{\mathtt{blade}} = E(1-0.025)$ and $E_{P_2}^{\mathtt{blade}} = E(1 + 0.015)$ (resp. $\mathbf{K}_{P_1}^{\mathtt{blade}} = \mathbf{K}^{\mathtt{blade}}(1 - 0.025)$ and $\mathbf{K}_{P_2}^{\mathtt{blade}} = \mathbf{K}^{\mathtt{blade}}(1 + 0.015)$), respectively.

For each (tuned or mistuned) case, the computed output response represents the absolute value of the tangential acceleration $\omega^2|q_\theta^{\mathtt{tip}}|$ of the tip of the blade of the substructure enclosed between the interfaces (N) and (1), see Fig. 4.

At first, the structure dynamics are assessed using a "reference" FE-based mode projection technique in the framework of which the displacement vector of a bladed disk is described using 359 vibration modes and 24 additional residual flexibility vectors to account for the excitation sources [14]. In this context, a reduced model of the whole structure is considered which is classically obtained by projecting, in the Galerkin sense, the mass, stiffness and damping matrices onto the space spanned by the vibration modes and the residual flexibility vectors. A sensitivity analysis can help select the number of vibration modes needed to obtain accurate dynamic responses on $[0\,,\,5000]$ Hz. Here, the selected modes are those for which the eigenfrequencies are below three times the maximum frequency of interest (i.e., below $15,000$ Hz). The mode projection technique leads to a structure model of small size which can be easily computed. The counterpart with this approach is the requirement to compute the vibration modes of a whole structure (offline task), and the fact that this step has to be repeated for each structure change considered (mistuning). This makes this technique less efficient compared to the WFE method.

Numerical simulations are carried out using MATLAB and in-house implementations of the proposed approaches. The reference response functions of the tuned and mistuned bladed disks are shown in Fig. 5. The response function of the tuned bladed disk reveals smooth behavior with a few resonance peaks over the frequency band analyzed. On the other hand, the response functions of the mistuned structures show many resonance peaks and, overall, complex response signals. For instance, the deformed shape of the tuned bladed disk for the resonance peak at 3020 Hz, and the deformed shapes of the mistuned bladed disks 1 and 2 for resonance peaks close to 3020 Hz (i.e., at 3027 Hz and 3012.5 Hz, respectively) are shown in Fig. 6. It is first noticed that the displacement field of the tuned structure is in agreement with the engine order excitation (EO $= 3$). Concerning the mistuned bladed disk 1, the perturbed substructure reveals high vibration levels compared to the neighbored substructures. In this sense, local resonant behavior occurs. As for the mistuned bladed disk 2, the energy localization effect is even more pronounced in the vicinity of the first perturbed substructure. In this case, the perturbed substructure as well as the two adjacent "safe" ones strongly vibrate.

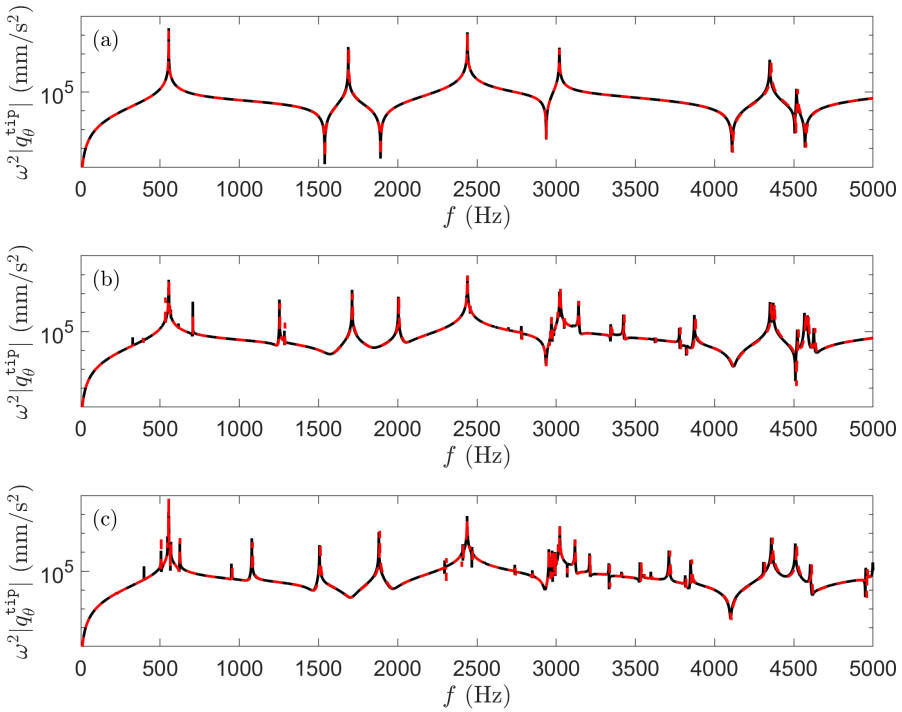

Figure 5: Response functions: (a) tuned bladed disk, (b) mistuned bladed disk 1 and (c) mistuned bladed disk 2: (black continuous line) reference; (red dashed line) WFE/reduction with $m = 120$.

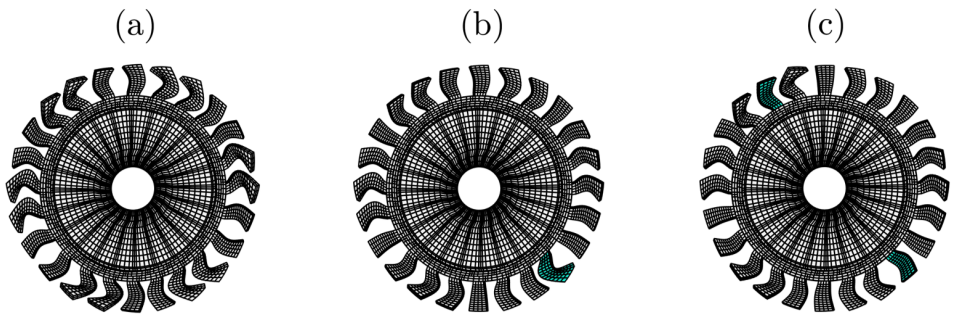

Figure 6: Deformed shapes: (a) tuned bladed disk at 3020 Hz, (b) mistuned bladed disk 1 at 3027 Hz and (c) mistuned bladed disk 2 at 3012.5 Hz. Perturbed blades are highlighted in green color (mistuned case).

Also the response functions of the tuned and mistuned bladed disks can be computed using the WFE method

and the reduction technique, see Secs. 2 and 3. First, a reduction of the number of internal DOFs of the substructures is performed, i.e., using $M_{\mathrm{I}} = 50$ fixed interface modes (see Sec. 3). Next, a reduction of the number of interface DOFs is performed, i.e., using m interface DOFs rather than $n = 726$ where $m < n$.

For instance, the error indicator $\mathcal{E}$, Eq. (47), can be assessed for $m = 20$, $m = 40$, $m = 60$, $m = 80$, $m = 100$ and $m = 120$ for the tuned and mistuned bladed disks. Especially, for each m, the maximum value of $\mathcal{E}$ over a coarse frequency grid with frequency step $\Delta f = 50$ Hz (up to 5000 Hz) can be assessed as shown in Fig. 7 where it is seen that the error can be strongly and quickly reduced for increasing m. For instance, $\mathcal{E} < 10\%$ for $m \geq 60$ and $\mathcal{E} < 5\%$ for $m \geq 100$. In order to compute accurate solutions, i.e., to accurately capture the local dynamics of the substructures at high frequencies, the choice is made here to express the response functions with $m = 120$, see Fig. 5. Here, the results issued from the proposed approach appear to be in good agreement with the reference ones over the whole frequency band of interest. Clearly this demonstrates the potential of the approach to handle the modeling and dynamic analysis of mistuned bladed disks.

In terms of efficiency, the computation of the dynamic responses of the mistuned bladed disk 1 requires roughly the same amount of time as the tuned structure. The analysis of the mistuned bladed disk 2 requires about $10 - 20\%$ additional times, which remains small. Although not done here, it seems that the analysis of bladed disks with more than two perturbed substructures could be efficiently done with the proposed approach.

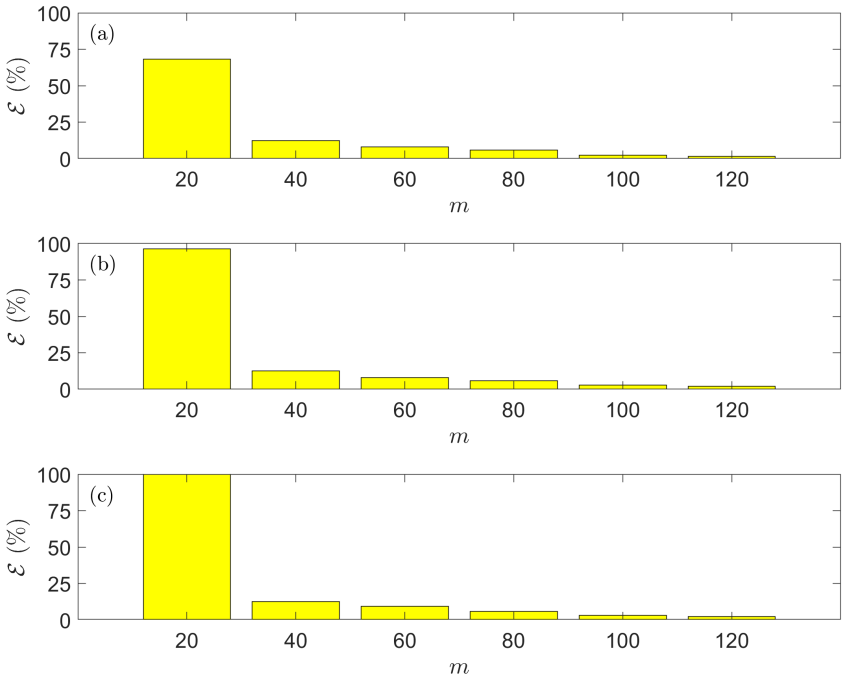

Figure 7: Error indicator $\mathcal{E}$ (maximum value within the frequency band of interest): (a) tuned bladed disk, (b) mistuned bladed disk 1 and (c) mistuned bladed disk 2.

5 Conclusion

The WFE method has been applied to compute the dynamic response of bladed disks with distributed loads (engine order excitation) where the focus is on the analysis of industrial structures with 3D substructures (sectors). To improve the efficiency of the WFE method, model reduction techniques have been proposed. To speed up, first, the computation of the condensed dynamic stiffness matrix of the substructures, a CB reduction for the internal DOFs has been proposed. Next, a second reduction for the interface DOFs has been

considered where the displacement vectors at the substructure interfaces are approximated with a reduced set of boundary modes. With this strategy, the computation of the wave modes can be drastically sped up. To control the accuracy of the model reduction techniques, an error indicator has been proposed. Numerical experiments have been conducted where the relevance of the WFE approach has been clearly highlighted for predicting the dynamic behavior of tuned and mistuned bladed disks.

Acknowledgments

This work has been funded by Safran.

References

[1] W. X. Zhong and F. W. Williams, "On the direct solution of wave propagation for repetitive structures," *Journal of Sound and Vibration*, vol. 181, no. 3, pp. 485–501, 1995.

[2] B. Mace, D. Duhamel, M. Brennan, and L. Hinke, "Finite element prediction of wave motion in structural waveguides," *Journal of the Acoustical Society of America*, vol. 117, pp. 2835–2843, 2005.

[3] J.-M. Mencik and M. Ichchou, "Multi-mode propagation and diffusion in structures through finite elements," *European Journal of Mechanics - A/Solids*, vol. 24, no. 5, pp. 877–898, 2005.

[4] Y. Waki, B. Mace, and M. Brennan, "Free and forced vibrations of a tyre using a wave/finite element approach," *Journal of Sound and Vibration*, vol. 323, no. 3-5, pp. 737–756, 2009.

[5] J.-M. Mencik, "A wave finite element approach for the analysis of periodic structures with cyclic symmetry in dynamic substructuring," *Journal of Sound and Vibration*, vol. 431, pp. 441–457, 2018.

[6] D. Beli, J.-M. Mencik, P. Silva, and J. Arruda, "A projection-based model reduction strategy for the wave and vibration analysis of rotating periodic structures," *Computational Mechanics*, vol. 62, pp. 1511–1528, 2018.

[7] T. Hoang, D. Duhamel, and G. Foret, "Wave finite element method for waveguides and periodic structures subjected to arbitrary loads," *Finite Elements in Analysis and Design*, vol. 179, p. 103437, 2020.

[8] T. Hoang, D. Duhamel, G. Foret, and L.-H. Tran, "Wave finite element method for the dynamics of structures with cyclic symmetry," *Proceedings of the 9th International Conference on Computational Methods in Structural Dynamics and Earthquake Engineering (COMPDYN), Athens, Greece*, 2023.

[9] R. Craig and M. Bampton, "Coupling of substructures for dynamic analyses," *AIAA Journal*, vol. 6, no. 7, pp. 1313–1319, 1968.

[10] D. Krattiger and M. Hussein, "Generalized bloch mode synthesis for accelerated calculation of elastic band structures," *Journal of Computational Physics*, vol. 357, pp. 183–205, 2018.

[11] M. Z. D. Krattiger, L. Wu, M. Buck, R. Kuether, M. Allen, P. Tiso, and M. Brake, "Interface reduction for hurty/craig-bampton substructured models: Review and improvements," *Mechanical Systems and Signal Processing*, vol. 114, pp. 579–603, 2019.

[12] J.-M. Mencik and D. Duhamel, "A wave-based model reduction technique for the description of the dynamic behavior of periodic structures involving arbitrary-shaped substructures and large-sized finite element models," *Finite Elements in Analysis and Design*, vol. 101, pp. 1–14, 2015.

[13] J.-M. Mencik, "New advances in the forced response computation of periodic structures using the wave finite element (wfe) method," *Computational Mechanics*, vol. 54, no. 3, pp. 789–801, 2014.

[14] F. Gruber and D. Rixen, "Evaluation of substructure reduction techniques with fixed and free interfaces," *Journal of Mechanical Engineering*, vol. 62, no. 7-8, pp. 452–462, 2016.